ADAPTIVE NUMERICAL TECHNIQUES FOR REACTIVE VAPOR INFILTRATION

S. Adjerid, J. E. Flaherty, M. S. Shephard, Y. J. Wang
Scientific Computation Research Center
W. Hillig, J. Hudson, N. Patibandla
Center for Composite Materials and Structures
Rensselaer Polytechnic Institute, Troy, New York 12180, USA

1. INTRODUCTION

Patibandla et al. [1,2] describe a reactive vapor infiltration (RVI) process for manufacturing fiber-reinforced ceramic composites where silicon carbide (SiC) or alumina (Al_2O_3) fibers are mixed with molybdenum (Mo) powder and pressed at room temperature to form a porous preform. The preform is exposed to a silicon tetra-chloride ($SiCl_4$) and hydrogen (H_2) flow where molecular-surface reactions liberate Si which, when absorbed into the preform, reacts with Mo to form a molybdenum di-silicide ($MoSi_2$) matrix. As a first step in modeling the RVI process, we present a mathematical model of the diffusion of Si into a compressed-powder Mo pellet to form the $MoSi_2$ matrix. The production of an intermediate (Mo_5Si_3) silicide layer, the growth of the $MoSi_2$ layer, and the volume expansion of the pellet are predicted. The model, consisting of a nonlinear ordinary and partial differential system, is solved using a state-of-the-art adaptive software system [3] that includes capabilities for automatic quadtree-structured mesh generation, mesh refinement/coarsening (h-refinement), method order variation (p-refinement), and mesh motion (r-refinement). Computational solutions of one- and two-dimensional problems indicate that the adaptive software is a robust and effective tool for addressing composite-processing problems. When compared with experimental observations, the mathematical model predicts a parabolic growth rate of the silicide layer and the volume expansion of the pellet to a high degree of accuracy. Anticipated applications of the adaptive software and enhancements to the mathematical model are described in a final section.

2. RVI MODEL

Patibandla et. al. [1,2] describe experiments where a pellet of a loosely compacted (45% porosity) Mo powder is subjected in a furnace to a flow of $SiCl_4$ and H_2 that reacts on the surface of grains of the pellet to liberate Si and hydrochloric acid (HCl). The Si is absorbed into the Mo pellet and reacts as

$$5Mo + 3Si \xrightarrow{k_1} Mo_5Si_3 \tag{2.1}$$

to form the silicide Mo_5Si_3, which quickly reacts as

$$Mo_5Si_3 + 7Si \xrightarrow{k_2} 5MoSi_2 \tag{2.2}$$

to form $MoSi_2$. These reactions occur in narrow fronts with free Si diffusing (principally by solid-state diffusion) through an $MoSi_2$ layer to reach the reaction zones.

The silicide-forming reactions (2.1,2) are accompanied by a 158% volume increase which fills the pores between grains of *Mo* powder, but may cause cracking [1,2].

Suppose the pellet contains a mixture of reactants and products and let the mass m_i (g) of species i at time t in a control volume V be

$$m_i = \int_V \rho Y_i \, dV, \quad i = 1, 2, 3, 4, \tag{2.3}$$

where ρ (g/cm^3) is the mixture density and Y_i, $i = 1, 2, 3, 4$, are, respectively, the mass fractions of Si, $MoSi_2$, Mo_5Si_3, and Mo. As the pellet deforms due to the volume change, we specify the position of each material point $\mathbf{x}$ as a function of t and its initial spatial position $\mathbf{X}$. With this reference, considerations of mass conservation for species i imply that

$$\frac{dm_i}{dt} = \int_{\partial V} \mathbf{J}_i \cdot \mathbf{n} \, d\sigma + \int_{\partial V} \rho Y_i \mathbf{v} \cdot \mathbf{n} \, d\sigma + \int_V \dot{r}_i \, dV, \quad i = 1, 2, 3, 4, \tag{2.4}$$

where $\dot{r}_i$ $(g/cm^3/sec)$ is the mass production rate and $\mathbf{J}_i$ $(g/cm^2/sec)$ is the diffusive flux of species i, ∂V is the boundary of V, $\mathbf{n}$ is the unit outer normal to ∂V, and

$$\mathbf{v}(\mathbf{X},t) = \partial_t \mathbf{x}(\mathbf{X},t) \tag{2.5}$$

is the mixture velocity.

Assuming Fickian diffusion

$$\mathbf{J}_i = -D_i \nabla(\rho Y_i), \tag{2.6}$$

with D_i (cm^2/sec) the diffusivity of species i in the mixture, applying the divergence theorem to (2.4), and using (2.3) yields the partial differential system

$$\frac{D(\rho Y_i)}{Dt} - \nabla \cdot D_i \nabla(\rho Y_i) + \rho Y_i \nabla \cdot \mathbf{v} = \dot{r}_i, \quad \mathbf{x} \in \Omega, \quad t > 0, \quad i = 1, 2, 3, 4, \tag{2.7a}$$

where

$$\frac{D}{Dt} = \partial_t + \mathbf{v} \cdot \nabla \tag{2.7b}$$

is the material derivative and Ω is the spatial region occupied by the pellet at time t.

Mass production rates are much faster than diffusion rates and, thus, cannot be observed. We assume that all reactions are irreversible and that they cease when one or more reactants are depleted. The form of the production rates should not significantly affect the results, so, for simplicity, we assume that they are linear in each concentration to obtain

$$\dot{r}_1 = -M_1(3w_1 + 7w_2), \quad \dot{r}_2 = 5M_2 w_2, \quad \dot{r}_3 = M_3(w_1 - w_2), \tag{2.8a,b,c}$$

$$\dot{r}_4 = -5M_4 w_1, \quad w_1 = k_1\left(\frac{\rho Y_1}{M_1}\right)\left(\frac{\rho Y_4}{M_4}\right), \quad w_2 = k_2\left(\frac{\rho Y_1}{M_1}\right)\left(\frac{\rho Y_3}{M_3}\right). \tag{2.8c,d,e}$$

The variables k_1 and k_2 (cm^3/sec) identify the rates of the reactions (2.1,2) and M_i (g) denotes the molecular weight of species $i = 1, 2, 3, 4$ (cf. Table I).

The process has been assumed to be isothermal, which should be acceptable since thermal variations produced by the reactions (2.1,2) have a negligible influence

at the temperature level of the furnace.

To include expansion, consider a volume V at time t where each chemical occupies the portion V_i, $i = 1, 2, 3, 4$. Letting V_0 denote the volume of the voids between chemical compounds, $\mu(\mathbf{x},t) = V_0/V$ denote the porosity, $\hat{\rho}_i = m_i/V_i$ (g/cm^3), $i = 1, 2, 3, 4$, denote species densities (cf. Table I), using (2.3), and letting V tend to zero gives

$$1 - \mu = \sum_{i=0}^{4} \frac{V_i}{V} = \sum_{i=1}^{4} \frac{m_i}{\hat{\rho}_i V} = \sum_{i=1}^{4} \frac{1}{\hat{\rho}_i V} \int_V \rho Y_i \, dV = \sum_{i=1}^{4} \frac{\rho Y_i}{\hat{\rho}_i}. \tag{2.9}$$

Table I. Molecular Weight M_i and Density $\hat{\rho}_i$ of Each Species.

i	1	2	3	4
Species	Si	$MoSi_2$	Mo_5Si_3	Mo
M_i	28	152	564	96
$\hat{\rho}_i$	2.34	6.24	7.38	10.2

Multiplying (2.7) by $1/\hat{\rho}_i$, summing over i, and using (2.9), we obtain

$$-\frac{D\mu}{Dt} + (\nabla\cdot\mathbf{v})(1 - \mu) = \sum_{i=1}^{4} \frac{1}{\hat{\rho}_i}[\dot{r}_i + \nabla\cdot D_i \nabla \rho Y_i], \quad \mathbf{x} \in \Omega, \quad t > 0. \tag{2.10}$$

The system is closed by assuming that the flow is irrotational ($\nabla \times \mathbf{v} = 0$) and by specifying a porosity function of the form $\mu(\mathbf{x}, t) = h(\rho, Y_1, \cdots, Y_4)$. Herein, we simplify (2.10) by neglecting μ, V_1/V, and the diffusive terms. As noted, μ is negligible in the silicide layer. Its effect in the unreacted mixture may be included in the densities of the initial components. With very little free Si in the pellet, it is reasonable to neglect its contribution to the total volume. The diffusivities D_2, D_3, and D_4 are negligible relative to D_1. With small Si concentrations, its diffusion may also be neglected when calculating the volume expansion. With these assumptions, (2.10) becomes

$$\nabla\cdot\mathbf{v} = \sum_{i=2}^{4} \frac{\dot{r}_i}{\hat{\rho}_i}. \tag{2.11}$$

Knowing the velocity divergence, we obtain the local volume change as

$$\frac{D(\det \mathbf{F})}{Dt} = (\det \mathbf{F})(\nabla\cdot\mathbf{v}) \tag{2.12}$$

where $\mathbf{F}$ is a matrix of the deformation gradients $\partial x_j/\partial X_k$, $j, k = 1, 2, 3$, and $\det \mathbf{F}$ is its determinant.

Specification of initial and boundary conditions complete the model (2.7,11,12). When, e.g., only Mo powder is present in the initial state, we prescribe

$$\rho(\mathbf{X},0) = \bar{\rho}, \quad Y_i(\mathbf{X},0) = 0, \quad i = 1, 2, 3, \quad Y_4(\mathbf{X},0) = 1, \quad \mathbf{v}(\mathbf{X},0) = 0, \quad \mathbf{X} \in \Omega \cup \partial\Omega, \tag{2.13}$$

where $\bar{\rho}$ is the initial mixture density.

Boundary conditions are developed by assuming that the reaction (2.1) ceases when a full monolayer of Si atoms is present on the surface. Therefore, the flux of Si atoms being absorbed into the pellet must equal the rate at which they are produced by the reaction (2.1). Moreover, we assume that the rate of absorption of Si atoms is proportional the deviation of Y_1 from the twice the maximum solubility S of Si in $MoSi_2$. Fluxes of other species through the boundaries are neglected; thus,

$$D_1\nabla(\rho Y_1)\cdot\mathbf{n} = -\alpha(Y_1 - S), \quad D_i\nabla(\rho Y_i)\cdot\mathbf{n} = 0, \quad i = 2, 3, 4, \quad \mathbf{x}\in\partial\Omega, \quad t > 0, \tag{2.14}$$

with $\alpha > 0$ and $S = 0.00037$.

3. COMPUTATIONAL RESULTS

We use an adaptive finite element software system with capabilities for automatic h-, p-, and/or r-refinement [3] to solve dimensionless versions of (2.7,8,11-14) in one and two spatial dimensions. With mesh motion, for example, we can both follow evolving fronts and track the volume expansion as the reaction progresses. The particular combination of h- and p-refinement is remarkably effective when high accuracy is necessary. Mesh refinement and order variation are controlled by a posteriori estimates of local discretization errors that have been either proven or observed to converge at the asymptotically correct rate for a wide range of problems [4]. Problems in this section were obtained by using an error indicator involving jumps in the first derivatives of the finite element solution across element boundaries [3,4]. Convergence of this indicator to the correct error is not known.

With the origin of a Cartesian coordinate system at the center of a $2a\times2b\times2c$ pellet, we introduce dimensionless variables with (x_1,x_2,x_3) scaled by (a,b,c), t scaled by $M_4/k_1\bar{\rho}$, and ρ scaled by $\bar{\rho}$. Employing symmetry, one-dimensional problems are solved on $0 < x_1 < a$ with x_2 and x_3 derivatives in (2.7,11-14) set to zero. Initially, we consider a problem involving a 45% porous Mo pellet. Selecting $a = 1\ mm$, $\alpha = 10^6\ (g/cm^2/sec)$, and $k_1 = 1.5\times10^3$ and $k_2 = 1.5\times10^2\ (g/cm^3)$, we solve problems with $D_1 = 0.37\times10^{-}5$, 1.5×10^{-5}, and $4.2\times10^{-5}\ (cm^2/sec)$ and $D_i = 10^{-20}\ (cm^2/sec)$, $i = 2, 3, 4$. The three values of D_1 correspond to observed diffusivities of Si at, respectively, temperatures of 1100, 1200, and 1300 ($°C$) [1,2].

We compare computed and observed [1,2] values for the square of the thickness of the $MoSi_2$ layer as a function of time for the three temperatures in the left portion of Figure 1. Computed and experimental results are in excellent agreement with deviations being less than 10%. Mass concentrations of $MoSi_2$, Mo_5Si_3, and Mo at a temperature of 1200 $°C$ and $t = 9.2\ hr$ are shown as a function of position in the right portion of Figure 1. The $MoSi_2$ layer is progressing from right to left in Figure 2; thus, the right-most curve is the mass fraction of $MoSi_2$, the steeply-peaked center curve is the mass fraction of Mo_5Si_3, and the left-most curve is the unreacted Mo. The thin Mo_5Si_3 layer moves with constant thickness as the reaction progresses, which agrees with observation [1].

Solutions shown in Figure 1 were obtained by hpr-refinement and in the left portion of Figure 2 we show the spatial mesh and method order used at 1200 $°C$ and $t = 9.2\ hr$. A coarse mesh and first-order method are used away from the reaction zone while finer meshes and high-order methods are used near the reaction. The mesh used to solve this problem is shown as a function of time in the right portion of

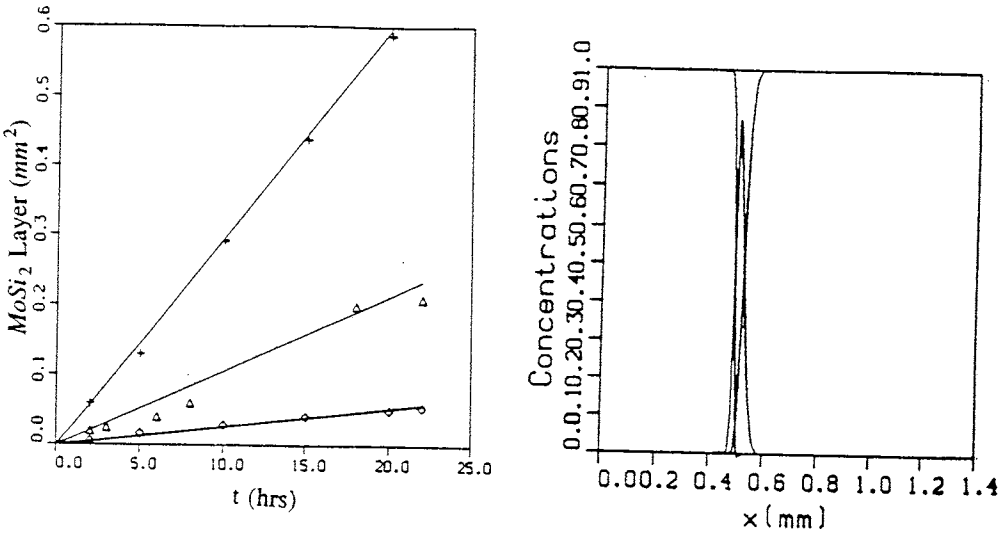

Figure 1. On the left, comparison of computed and observed values of the square of the thickness of the $MoSi_2$ layer as a function of time for temperatures of 1100 °C (triangles), 1200 °C (plusses), and 1300 °C (diamonds). On the right, mass fractions of $MoSi_2$, Mo_5Si_3, and Mo at 1200 °C and t = 9.2 hr as a function of position.

Figure 3. The mesh is concentrated near the front and moving to account for the expansion as the reaction occurs.

Production times can be reduced by starting with a mixture of Mo and $MoSi_2$ [2]. We compare computed and observed [2] values for the square of the thickness of the $MoSi_2$ layer as a function of time in the left portion of Figure 3. Initial concentrations consisted of all Mo; 50% Mo and 50% $MoSi_2$; and 30% Mo and 70% $MoSi_2$. Corresponding diffusivities of Si in the mixture were $D_1 = 1.5\times10^{-5}$, 3.08×10^{-5}, and 3.08×10^{-5} (cm^2/sec). The reaction temperature was 1200 °C and all other parameters were as specified in the previous computation. Computationally, we assume that the initial Mo-$MoSi_2$ mixture quickly reacts to form Mo_5Si_3 with an excess of either Mo or $MoSi_2$ according to the phase equilibrium diagram. In particular, the 50% Mo-$MoSi_2$ mixture reacts to form all Mo_5Si_3 at a 61% porosity and we use this as an initial state with the software. With 30% Mo and 70% $MoSi_2$, we begin with an initial state of 52% Mo_5Si_3 and 48% $MoSi_2$.

On the right of Figure 3, we present the relative change in volume as a function of time with initial concentrations of all Mo at 45% porosity and 50% Mo and 50% $MoSi_2$ at 45% porosity. In order to give some indication of the effects of porosity, we also present the volume expansion corresponding to an initial dense state of all Mo. Production times are fastest with an initial mixture of 30% Mo and 70% $MoSi_2$ because of the need to diffuse less Si and the doubling of the diffusivity with the Mo-$MoSi_2$ mixture. This latter effect is not understood at this time. Volume expansion with the dense Mo initial state is excessive and can result in cracking. Starting

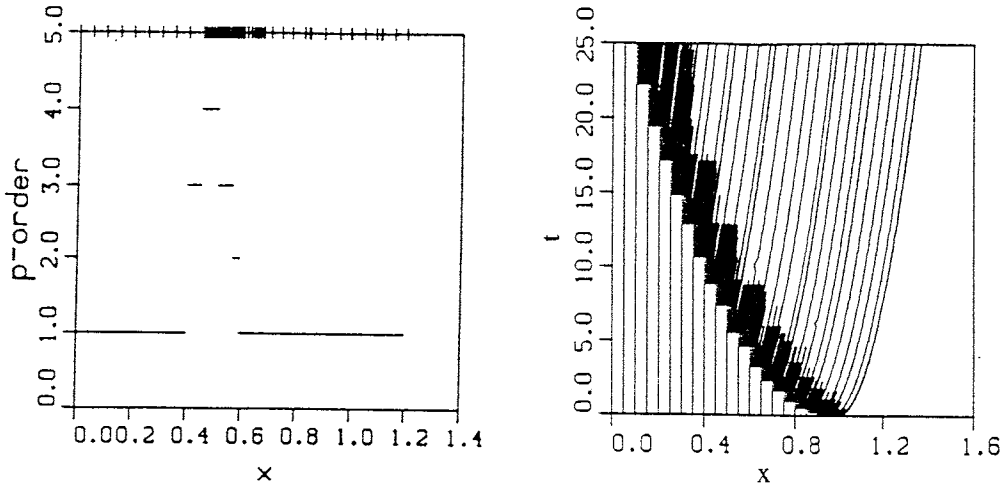

Figure 2. Method order and spatial mesh (left) and mesh position as a function of time (right).

with an initial Mo-$MoSi_2$ mixture effectively eliminates expansion and will, hence, result in a more predictable matrix geometry.

To further illustrate the capabilities of our software, we solved (2.7,8,11-14) in two spatial dimensions for a pellet with $a = 0.5\ mm$ and $b = 0.125\ mm$ having an initial Mo concentration at 45% porosity. The remaining parameters were the same as in the one-dimensional examples with a temperature of 1200 $°C$. For simplicity, the boundary condition (2.14a) was replaced by the Dirichlet condition $\rho Y_1 = 1.58 S \bar{\rho}$. In Figure 4, we present the mass concentration of $MoSi_2$ at 14.3 hours obtained using piecewise linear finite element approximations with adaptive h-refinement on a mesh of triangular elements. With symmetry, we have displayed the solution in a portion of a quadrant of the pellet's cross section. Shading in Figure 4 is proportional to the concentrations of $MoSi_2$ with darker shading indicating higher concentrations. At the instant of time shown, the software has anticipated the inward propagation of the reaction zone and has concentrated the mesh towards the leading edge of the front.

4. DISCUSSION

We have developed a reaction-diffusion system to analyze the RVI process of fabricating ceramic composites. When used with an adaptive finite element software system [3], the model predicted the growth of an $MoSi_2$ layer in a siliciding application [1,2]. Production rates, volume expansion, and other effects may be studied as functions of, e.g., initial composition and porosity. The one- and two-dimensional adaptive software systems [3,4] have a symbolic interface that makes it easy to change models either to include more complex and realistic effects or to study other similar processes.

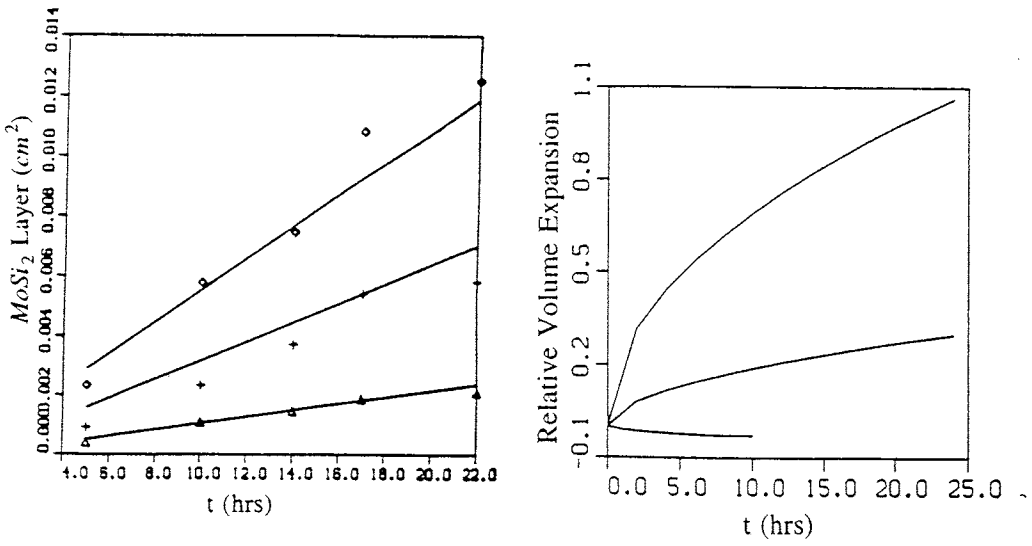

Figure 3. On the left, comparison of computed and observed values of the square of the thickness of the $MoSi_2$ layer as a function of time for initial concentrations of all *Mo* (triangles); 50% *Mo* and 50% $MoSi_2$ (plusses); and 30% *Mo* and 70% $MoSi_2$ (diamonds) at 45% porosity. On the right, relative change in volume as a function of time for initial concentrations of all *Mo* with no porosity, all *Mo* at 45% porosity, and 50% *Mo* and 50% $MoSi_2$ at 45% porosity (top to bottom).

As *Mo* grains react to form $MoSi_2$, they swell to close pores and voids between them and, eventually, exert forces on neighboring grains. The initial effect reduces or eliminates fluid infiltration into the pellet and establishes solid-state diffusion as the dominant transfer mechanism. The latter effect creates a stress field that may induce cracking [2] or residual stresses. Pores close quickly to choke fluid access with the present initial porosities; however, we intend to model this process at the granular level to better understand the effects of initial packing densities. Our software is capable of solving these fluid-solid interaction problems with varying geometries and, if not useful in our RVI application, it may be used to address other chemical vapor infiltration applications [5]. More realistic surface reaction models between solid and fluid phases will be introduced at this stage.

Even without gaseous infiltration, it is important to understand the closing of pores in the interior of the pellet to ensure that the matrix material has a homogeneous structure and chemistry. This can be studied at the macroscopic level using the model (2.7,8,11-14); however, a preliminary study at the granular level is necessary to, at least, identify an appropriate porosity function $\mu(\mathbf{x},t)$ and other effective properties for granular materials. Combined mechanical and chemical processing models will be subsequently developed with a goal of predicting cracking and residual stresses.

Future experiments will be performed with fibers embedded in a powder preform and our models will be modified to reflect this. Our investigation will seek to reveal

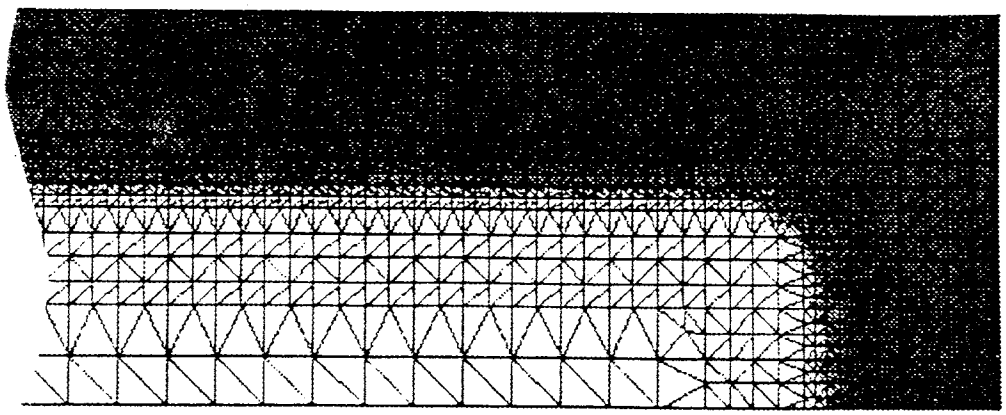

Figure 4. Mass fraction of $MoSi_2$ in a portion of a quadrant of a two-dimensional cross section of the pellet. Darker colors indicate higher concentrations of $MoSi_2$.

optimal fiber placements, packing densities, and process strategies. By combining a computational and experimental program we are able to identify and verify prototypical optimal combinations much more rapidly than would be possible by using either paradigm alone.

ACKNOWLEDGMENT

The authors gratefully acknowledge support of this project from ARPA/ONR under grant N00014-92J-1779 "Mechanism-Based Design of Composite Structures," Steven Fishman and William Coblenz, Project Monitors.

References

1. N. Patibandla and W.B. Hillig, Processing of Molybdenum Di-silicide Using a New Reactive Vapor Infiltration Technique, *J. Am. Ceram. Soc.*, **76**, pp. 1630-1634, 1993.

2. N. Patibandla, W.B. Hillig, and M.R. Ramakrishnan, *SiC* Fiber Reinforced $MoSi_2$ Matrix Composites Produced Via Reactive Vapor Infiltration, preprint, Center for Composite Materials and Structures, Rensselaer Polytech. Inst., 1993.

3. S. Adjerid, J.E. Flaherty, P.K. Moore, and Y.J. Wang, High-Order Methods for Parabolic systems, *Physica D,* **60**, pp. 94-111, 1992.

4. S. Adjerid and J.E. Flaherty, and Y. J. Wang, A Posteriori Error Estimation with Finite Element Methods of Lines For One-Dimensional Parabolic Systems, *Numer. Math.*, **65**, pp. 1-21, 1993.

5. N.H. Thai and T.W. Chou, Modelling of an Improved Chemical Vapor Infiltration Process for Ceramic Composites Fabrication, *J. Am. Ceram. Soc.*, **73**, pp. 1489-1498, 1990.